




Frequency and power stabilization of a terahertz quantum-cascade laser using near-infrared optical excitation

T. ALAM,^{1,*} M. WIENOLD,^{1,2} X. LÜ,³ K. BIERMANN,³ L. SCHROTTKE,³  H. T. GRAHN,³ AND H.-W. HÜBERS^{1,2}

¹German Aerospace Center (DLR), Institute of Optical Sensor Systems, Rutherfordstr. 2, 12489 Berlin, Germany

²Humboldt-Universität zu Berlin, Department of Physics, Newtonstr. 15, 12489 Berlin, Germany

³Paul-Drude-Institut für Festkörperelektronik, Leibniz-Institut im Forschungsverbund Berlin e. V., Hausvogteiplatz 5–7, 10117 Berlin, Germany

*tasmim.alam@dlr.de

Abstract: We demonstrate a technique to simultaneously stabilize the frequency and output power of a terahertz quantum-cascade laser (QCL). This technique exploits frequency and power variations upon near-infrared illumination of the QCL with a diode laser. It does not require an external terahertz optical modulator. By locking the frequency to a molecular absorption line, we obtain a long-term (one-hour) linewidth of 260 kHz (full width at half maximum) and a root-mean-square power stability below 0.03%. With respect to the free-running case, this stabilization scheme improves the frequency stability by nearly two orders of magnitude and the power stability by a factor of three.

© 2019 Optical Society of America under the terms of the [OSA Open Access Publishing Agreement](#)

1. Introduction

Terahertz (THz) quantum-cascade lasers (QCLs) are of great importance as local oscillators (LOs) for high-resolution heterodyne spectroscopy above 3 THz [1–3]. Heterodyne receivers are commonly used for astronomical and atmospheric observations in the THz range [4]. The frequency resolution and radiometric accuracy of such a system depend on the frequency and output power stability of the LO. Increasing the stability of the LO with respect to frequency and output power has a direct impact on the performance of a heterodyne receiver. Recent studies have shown that the intrinsic quantum limit for the linewidth of THz QCLs lies in the sub-kHz range [5,6]. However, the practical linewidth for a free-running THz QCL is much larger, which is due to the limited stability of the driving current and temperature as well as to optical feedback [7]. In practice, the emission frequency drift can exceed 10 MHz [8,9]. Stabilizing the frequency and output power becomes even more challenging when the QCL is operated in a mechanical cryocooler, where vibration noise is intrinsically present. For these reasons, there has been a significant interest in improving both, the output power and frequency stability. To date, several techniques have been demonstrated for frequency stabilization. Among them are phase locking to a frequency multiplied microwave source [10–12] or a THz frequency comb [13,14], locking to a THz gas laser [15,16], and injection locking of a QCL to a telecommunication frequency comb [17]. An alternative method, which has been well established for diode lasers, is the stabilization to an atomic or molecular absorption line to achieve absolute long-term stability of the laser frequency [18,19]. This approach has also been demonstrated for QCLs [20,21]. For a simultaneous output power control of a frequency-stabilized THz QCL, a swing-arm voice coil actuator has been used as a fast optical attenuator [22]. Recently, amplitude stabilization of a 2.85-THz QCL has been achieved with a graphene-loaded, split-ring-resonator array acting as an external amplitude modulator. In this case, the transmittance of the modulator was controlled

by modifying the graphene conductivity via electrostatic back gating [23]. In the following sections, we describe a method that allows for a simultaneous stabilization of the frequency and output power by taking advantage of the frequency and power regulation by near-infrared (NIR) excitation [24,25] in addition to frequency and power control by the modification of the driving current so that no external THz optical modulator is required.

2. Experimental setup

The experimental configuration is shown as a schematic diagram in Fig. 1(a). The QCL used in our experiment is based on a GaAs/Al_{0.18}Ga_{0.82}As active-region structure [26] with a single-plasmon waveguide. It is an uncoated Fabry-Pérot device, 120 μm wide and 660 μm long, and exhibits single-mode emission at 3.1 THz. The same laser was used to demonstrate molecular spectroscopy by light-induced frequency tuning [25]. The QCL is operated in a mechanical cryocooler (Ricor, model K535), and the temperature is stabilized at 45 K. The exit window of the cooler is made of high-density polyethylene (HDPE). A poly-4-methylpentene-1 (TPX) lens collimates the QCL beam, and a Mylar beam splitter divides the beam into two parts, where the reflected beam is used for power stabilization, while the transmitted beam passes through a methanol (CH₃OH) gas cell for frequency locking to a molecular absorption line. Two helium-cooled Ge:Ga detectors (labeled A and B) are used to measure the transmitted and the reflected signals. A single-mode NIR diode laser (Lumics, LU0808M250) is used as a source for illuminating the rear facet of the THz QCL. The diode laser emits 200 mW of optical power into a polarization-maintaining single-mode fiber with a core diameter of 4.5 μm and a numerical aperture (NA) of 0.12. The fiber is clamped to a linear stepper positioner (Attocube, ANPx51) driven by a motion controller (Attocube, ANC 300) to allow for the lateral alignment of the NIR spot on the QCL chip. Since the fiber is attached to the cold finger as shown in Fig. 1(b), cooler vibrations do not have an impact on the alignment as compared to our microscope technique described in [25]. The DC current for the QCL is provided by the driver QCL1000 LAB (Wavelength Electronics). The driver has a typical modulation bandwidth of up to 3 MHz and a modulation coefficient of 200 mA/V.

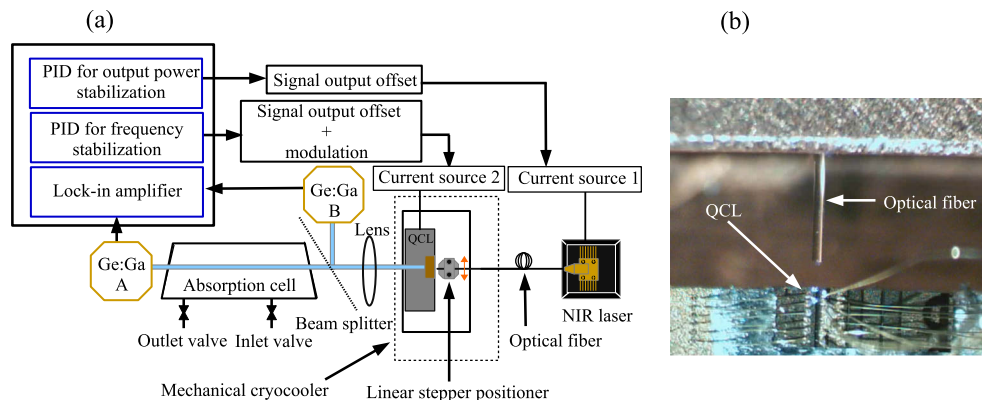


Fig. 1. (a) The schematic diagram of the setup used to stabilize the frequency and output power. The QCL is operated in a mechanical cryocooler. The combination of the absorption cell and the Ge:Ga detector A is used to lock the frequency, and the second Ge:Ga detector B is used as a reference for the output power stabilization. (b) Rear-facet illumination with a low-NA single-mode fiber.

3. Frequency tuning measurements

To identify a frequency range suitable for stabilization, we investigate the absorption characteristics of CH_3OH at 3.1 THz using two different tuning methods. First, we measured the absorption spectrum as a function of the QCL current from 250 to 380 mA at a temperature of 45 K, while the NIR diode laser was switched off. Figure 2(a) shows the resulting spectrum as a function of the driving current exhibiting seven absorption lines. Second, light-induced frequency tuning was performed, for which the QCL is operated at a constant driving current and the laser diode current is ramped from below threshold up to 370 mA. The corresponding absorption signal after a fourth-order polynomial baseline subtraction is shown in Fig. 2(b). The individual lines of the CH_3OH spectral fingerprint are identified with the help of the Jet Propulsion Laboratory (JPL) molecular catalog [27]. With such a frequency calibration, the tuning behavior can be precisely recovered. By changing the QCL driving current, we achieved a frequency coverage of about 2.5 GHz [cf. inset of Fig. 2(a)]. To a reasonable approximation, the QCL frequency depends linearly on the QCL current as well as on the heat sink temperature (not shown). For the used laser, we identified a suitable single-mode frequency range of 3.1455–3.148 THz. In the case of diode laser tuning, we found that the QCL frequency shift follows a square root behavior with increasing diode laser current above threshold. Details of this method can be found in [25]. In this tuning mode, a frequency coverage of about 8 GHz [cf. inset of Fig. 2(b)] was achieved with only 200 mW of optical power.

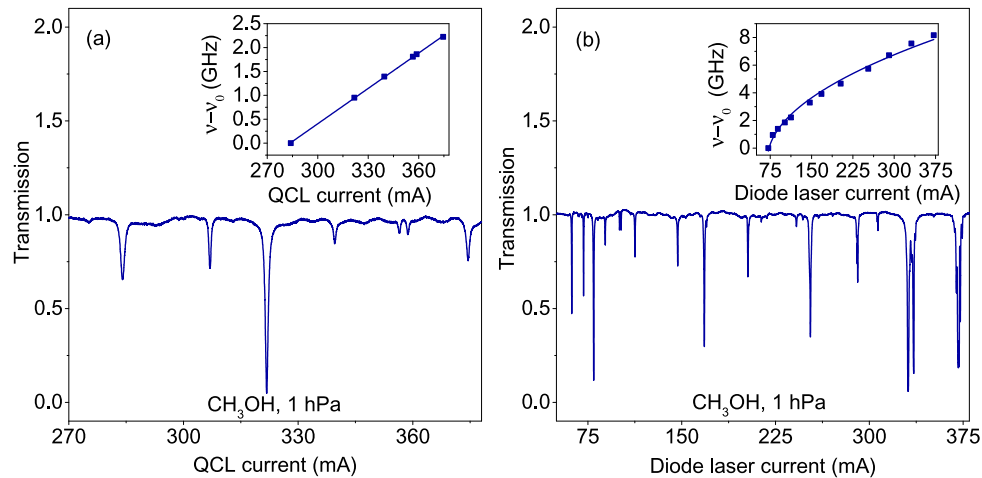


Fig. 2. Absorption spectra of CH_3OH in a 60-cm cell, at a pressure of 1 hPa and heat sink temperature of 45 K, (a) by varying the QCL driving current and (b) by varying the diode laser intensity. The insets in (a) and (b) depict the derived frequency (ν) tuning characteristics, where the solid lines refer to a linear and a square-root data fit, respectively, and $\nu_0 = 3.14589$ THz.

4. Frequency modulation spectroscopy

In order to lock the frequency to a molecular absorption line, a distinctive signal is required for the control loop, which contains information about the magnitude and the direction of the frequency deviation. Therefore, a small sinusoidal modulation at 1 MHz is added with a bias-tee to the QCL driving current, and the detector signal after an absorption cell is recorded with a lock-in amplifier (Zurich Instruments, UHFLI). This frequency modulation (1f) results in a derivative-like absorption signal. At the same time, it provides phase and amplitude information corresponding

to the direction and magnitude, respectively, of the required corrections. Figure 3(a) shows the derivative-like absorption spectrum of CH_3OH at a pressure of 1.5 hPa. Each line can be used to provide an error signal for the QCL frequency locking. In this experiment, the QCL current is tuned from below threshold over the whole range of single-mode operation, resulting in acquisition times of 50–100 ms/scan. All signals are acquired with a fast data acquisition device (CDAQ, National Instruments), where both, the input and output channels, are synchronized with the lock-in amplifier at a clock rate of 10 MHz.

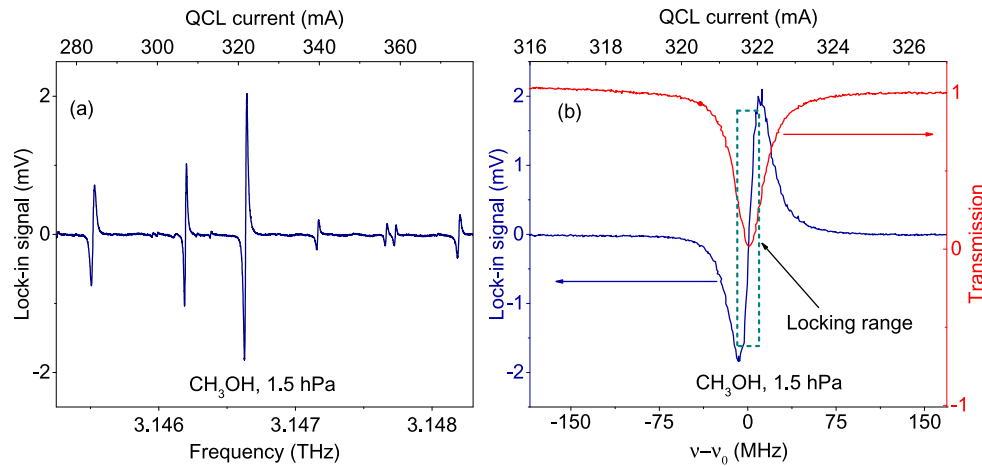


Fig. 3. (a) Derivative-like absorption spectrum of CH_3OH for a modulation frequency of 1 MHz, a cell length of 60 cm, a pressure of 1.5 hPa, and a heat sink temperature of 45 K. (b) Absorption line of CH_3OH for a pressure of 1.5 hPa, where $\nu_0 = 3.14685$ THz. The transmission signal is measured in direct detection, while the frequency-modulated signal is measured with the lock-in amplifier. The locking range is indicated by the rectangular box.

5. Frequency and output power stabilization

Figure 3(b) shows the CH_3OH absorption line at 3.14685 THz and the corresponding derivative-like signal, which will be used for the frequency stabilization. The absorption signal is measured directly with the Ge:Ga detector through a variation of the QCL driving current at a pressure of 1.5 hPa and the frequency-modulated signal is measured with the lock-in amplifier. The derivative-like signal changes linearly with the QCL driving current close to the center of the absorption line. Therefore, the error signal can be converted directly into a frequency scale. The linear range of the error signal also indicates the locking range of the control loop. We only used the proportional and integral parameters of the proportional-integral-derivative (PID) controller for the frequency locking. The proportional gain corrects the error in a small time interval, and the integral part accumulates the error over time and is used to correct a possible residual offset. The controller provides feedback to the QCL driving current to keep its frequency aligned with the center of the absorption line.

A second feedback loop is used to achieve amplitude stabilization by varying the diode laser driving current, where the signal of the Ge:Ga detector B is used as a reference for the QCL power level. The deviation of the power signal from a predefined set point is used as an error signal. By combining both control loops, the QCL frequency and power level can be stabilized without the need for an external THz modulator. To characterize the stabilization approach, we monitor the fluctuations of the frequency and output power of the QCL for different cases. Figures 4(a) and 4(b) show the frequency and output power stability, respectively, for (1) the

free-running QCL, (2) the frequency-locked QCL, and (3) the frequency- and power-locked QCL. In the free-running case, the rather strong frequency and amplitude fluctuations are correlated with the cooler vibrations (45-Hz cycle of the piston). In the second case when the frequency stabilization loop is enabled, the frequency becomes well stabilized, but fluctuations in the QCL output power increase. In the third case, when both control loops are activated simultaneously, the power and frequency remain stable at the expense of a very small increase of the frequency noise level. In Fig. 4(c), the noise signal from detector A is shown together with the error signal for the stabilized QCL. The noise level was measured by blocking the QCL radiation in front of the detector. This illustrates that the QCL frequency stabilization operates already close to the detector noise limit.

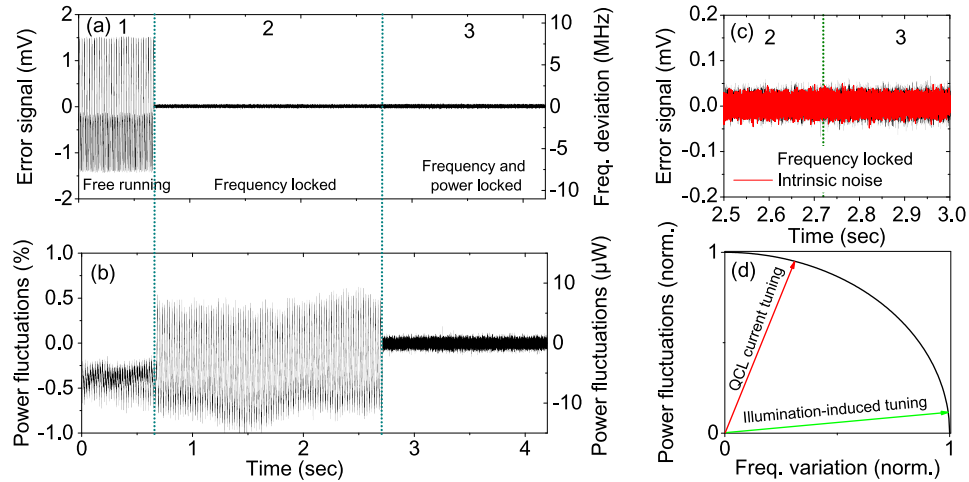


Fig. 4. (a) Frequency stability versus time detected by the lock-in amplifier in the locking range indicated in Fig. 3(b). (b) DC output of detector B reflecting the QCL output power versus time. Three different cases are shown: (1) free running, (2) frequency stabilized, and (3) both, frequency and amplitude, stabilized. (c) Magnified region around 2.7 sec showing the frequency-locked signal in comparison to the detector noise level. (d) Normalized tuning vectors for the QCL current and the diode laser tuning.

To explain the anti-correlation between frequency and output power stability in the second case, we need to discuss the impact of the control parameters on the QCL behavior. As discussed in [25], the QCL frequency and the output power depend on three control parameters: the QCL driving current, the heat sink temperature, and the diode laser excitation power. The temperature control is typically too slow for an active stabilization. Since the control parameters simultaneously affect the QCL frequency and output power, stabilizing one quantity will result in increased fluctuations of the other one. Simultaneous frequency and power stabilization therefore requires two separate control loops operating at the same speed. Another requirement is that the ratio of the power-to-frequency tuning must differ for the two control parameters. This is in analogy to the requirement of two linear independent base vectors to span a two-dimensional phase space. With the help of the tuning coefficients, we can define a pair of tuning vectors α_I and α_L for current and illumination tuning, respectively, at the particular operating point chosen in Fig. 4 for stabilization. For QCL current tuning, $\alpha_I = (+24.65 \text{ MHz/mA}, +13.7 \text{ } \mu\text{W/mA})$, while for illumination tuning $\alpha_L = (+59.4 \text{ MHz/mA}, -1.25 \text{ } \mu\text{W/mA})$. Eventually the frequency

and power variations are described by the equation

$$\begin{pmatrix} \Delta v \\ \Delta P \end{pmatrix} = \Delta I_{\text{QCL}} \alpha_I + \Delta I_{\text{DL}} \alpha_L. \quad (1)$$

In order to compare the vector for current tuning with the one for illumination tuning, we divide the tuning vectors by the free-running root-mean-square (rms) fluctuations of 6.2 MHz and 1.6 μW , respectively, with the latter one corresponding to about 0.1% of the QCL power of 1.5 mW. We further obtain dimensionless tuning vectors by normalizing their length to unity, because the actual value of the control parameter is not important here. The resulting normalized tuning vectors are shown in Fig. 4(d). In the present case, they span an angle of about 65° in the corresponding normalized phase space. For minimizing crosstalk effects, the tuning vectors should be ideally orthogonal and aligned along the frequency and power axis. In theory, such a pair of orthogonal tuning vectors can be obtained by a simple base transformation. A real-time implementation of such an improved PID loop may be realized with the help of a controller based on a field-programmable gate array.

Figure 5 depicts the frequency and output power distributions for the free-running and stabilized cases shown in Fig. 4. Figure 5(a) depicts a histogram of the frequency fluctuations for the free-running state. The distribution spans almost 20 MHz, and its non-Gaussian shape is a consequence of the periodic cooler vibrations. The width of the distribution has to be considered as a lower limit since it exceeds the linear range of the error signal. For the frequency-locked state shown in Fig. 5(b), the distribution exhibits a Gaussian line shape with a full width at half maximum (FWHM) of 240 kHz, and, for the fully locked state, the line shape corresponds to a FWHM of 260 kHz shown in Fig. 5(c). For comparison, the noise level of detector A as shown in Fig. 4(c) corresponds to a Gaussian line shape with a FWHM of 200 kHz. These values indicate that the intrinsic noise level of the detector contributes significantly to the line width of the stabilized QCL. Figures 5(d), 5(e), and 5(f) compare the power stability for the cases of the free-running, frequency-locked, and fully stabilized QCL, respectively. The fluctuations amount to 0.1% (rms) in the free-running case. For the frequency-locked case without power stabilization, the output power fluctuations of the QCL increased to about 0.4% (rms). When both, the amplitude and frequency stabilization loops are active, the output power becomes well stabilized, and the fluctuations are reduced to 0.03% (rms), corresponding to a Gaussian

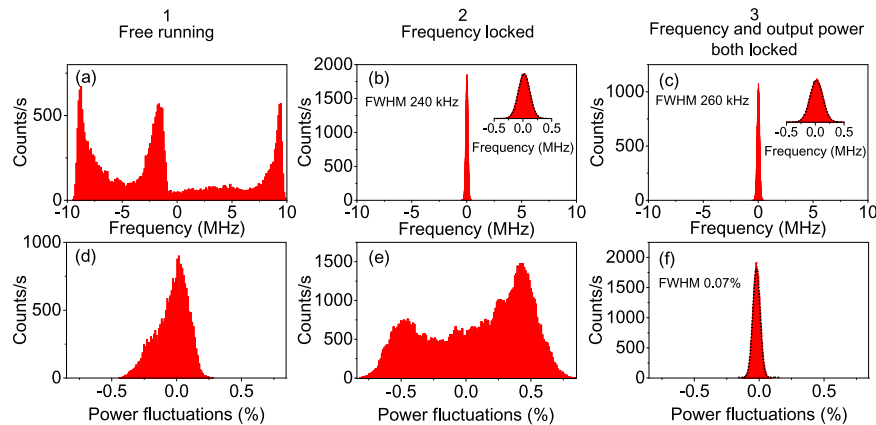


Fig. 5. Histograms of the (a)–(c) frequency and (d)–(f) power fluctuations corresponding to the unlocked state and the locked states shown in Fig. 4. Dotted lines refer to a normal distribution.

distribution with a FWHM of 0.07%. This is a more than three-fold improvement with respect to the unstabilized case.

We also carried out a long-term stability test by locking both, frequency and power, over one hour. In order to illustrate the impact of the cooler vibrations and the control loop action, Figs. 6(a) and 6(b) depict the power spectral density (PSD) for the frequency and the amplitude noise, respectively, for the three situations shown in Fig. 4. The noise PSD corresponds to the magnitude squared of the Fourier-transformed frequency and amplitude fluctuations. Note that the square root of the integrated PSD must be equal to the rms standard deviation of the corresponding distribution. For a Gaussian distribution, this is equal to the FWHM value divided by 2.355. For the free-running case, the PSDs of the frequency and amplitude noise are clearly dominated by the cooler vibrations at 45 Hz and higher harmonics. These contributions become suppressed in the frequency noise as soon as the frequency stabilization loop is activated. However, they become more pronounced in the amplitude noise due to a significant power component of the tuning vector. After activating the second control loop, they are also suppressed in the PSD of the amplitude noise at the expense of a somewhat increased noise at high frequencies, which we attribute to the crosstalk between the control loops by the non-orthogonal tuning vectors.

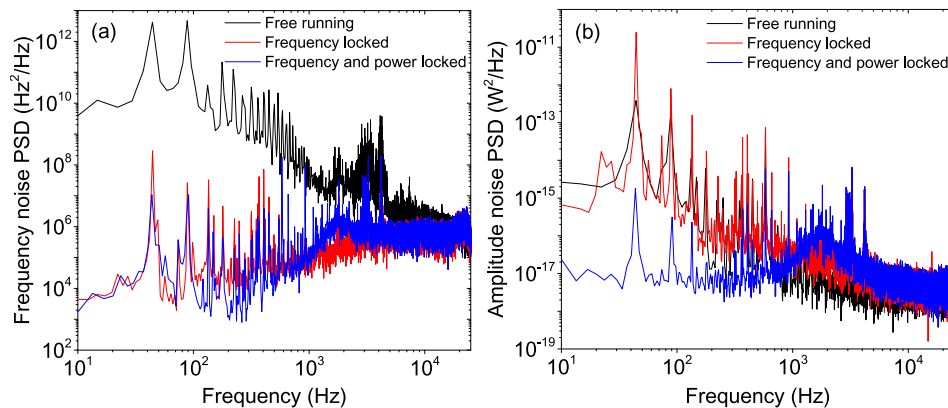


Fig. 6. PSD of the (a) frequency noise and (b) amplitude noise for the free-running, the frequency-locked, and the frequency and power-locked QCL. The bandwidth of the PID control loops for frequency and output power stabilization is 193 kHz and 1.7 kHz, respectively.

6. Conclusion

We successfully demonstrated the simultaneous stabilization of frequency and output power of a THz QCL operated in a compact cryocooler. Frequency stabilization is achieved by locking the QCL to a CH₃OH absorption line. Frequency and output power are adjusted via the QCL driving current and the NIR laser excitation of the QCL rear facet, which act as two independent control parameters. The setup is compact and robust due to the direct coupling of the illumination through an optical fiber. No external THz optical modulator is required to regulate the frequency and output power. This scheme could play a vital role in improving the performance of high-resolution spectroscopic systems.

Acknowledgments

The authors would like to thank H. Richter for fruitful discussions on the method of frequency stabilization and W. Anders, M. Hörnicke, A. Riedel, and A. Tahraoui for sample preparation. T. Alam acknowledges the support by the Helmholtz Research School on Security Technologies.

Disclosures

The authors declare that there are no conflicts of interest related to this article.

References

1. H. Richter, M. Wienold, L. Schrottke, K. Biermann, H. T. Grahn, and H.-W. Hübers, "4.7-THz Local Oscillator for the GREAT Heterodyne Spectrometer on SOFIA," *IEEE Trans. Terahertz Sci. Technol.* **5**(4), 539–545 (2015).
2. C. Risacher, R. Güsten, J. Stutzki, H.-W. Hübers, D. Büchel, U. U. Graf, S. Heyminck, C. E. Honingh, K. Jacobs, B. Klein, T. Klein, C. Leinz, P. Pütz, N. Reyes, O. Ricken, H.-J. Wunsch, P. Fusco, and S. Rosner, "First Supra-THz Heterodyne Array Receivers for Astronomy With the SOFIA Observatory," *IEEE Trans. Terahertz Sci. Technol.* **6**(2), 199–211 (2016).
3. H.-W. Hübers, H. Richter, and M. Wienold, "High-resolution terahertz spectroscopy with quantum-cascade lasers," *J. Appl. Phys.* **125**(15), 151401 (2019).
4. C. Risacher, R. Güsten, J. Stutzki, H.-W. Hübers, R. Aladro, A. Bell, C. Buchbender, D. Büchel, T. Csengeri, C. Duran, U. U. Graf, R. D. Higgins, C. E. Honingh, K. Jacobs, M. Justen, B. Klein, M. Mertens, Y. Okada, A. Parikka, P. Pütz, N. Reyes, H. Richter, O. Ricken, D. Riquelme, N. Rothbart, N. Schneider, R. Simon, M. Wienold, H. Wiesemeyer, M. Ziebart, P. Fusco, S. Rosner, and B. Wohler, "The upGREAT Dual Frequency Heterodyne Arrays for SOFIA," *J. Astron. Instrum.* **07**(04), 1840014 (2018).
5. M. S. Vitiello, L. Consolino, S. Bartolini, A. Taschin, A. Tredicucci, M. Inguscio, and P. De Natale, "Quantum-limited frequency fluctuations in a terahertz laser," *Nat. Photonics* **6**(8), 525–528 (2012).
6. M. Ravaro, S. Barbieri, G. Santarelli, V. Jagtap, C. Manquest, C. Sirtori, S. P. Khanna, and E. H. Linfield, "Measurement of the intrinsic linewidth of terahertz quantum cascade lasers using a near-infrared frequency comb," *Opt. Express* **20**(23), 25654–25661 (2012).
7. H.-W. Hübers, H. Richter, R. Eichholz, M. Wienold, K. Biermann, L. Schrottke, and H. T. Grahn, "Heterodyne Spectroscopy of Frequency Instabilities in Terahertz Quantum-Cascade Lasers Induced by Optical Feedback," *IEEE J. Sel. Top. Quantum Electron.* **23**(4), 1–6 (2017).
8. A. Barkan, F. K. Tittel, D. M. Mittleman, R. Dengler, P. H. Siegel, G. Scalari, L. Ajili, J. Faist, H. E. Beere, E. H. Linfield, A. G. Davies, and D. A. Ritchie, "Linewidth and tuning characteristics of terahertz quantum cascade lasers," *Opt. Lett.* **29**(6), 575–577 (2004).
9. S. Barbieri, J. Alton, H. E. Beere, E. H. Linfield, D. A. Ritchie, S. Withington, G. Scalari, L. Ajili, and J. Faist, "Heterodyne mixing of two far-infrared quantum cascade lasers by use of a point-contact Schottky diode," *Opt. Lett.* **29**(14), 1632–1634 (2004).
10. P. Khosropanah, A. Baryshev, W. Zhang, W. Jellema, J. N. Hovenier, J. R. Gao, T. M. Klapwijk, D. G. Paveliev, B. S. Williams, S. Kumar, Q. Hu, J. L. Reno, B. Klein, and J. L. Hesler, "Phase locking of a 2.7 THz quantum cascade laser to a microwave reference," *Opt. Lett.* **34**(19), 2958–2960 (2009).
11. D. Rabanus, U. U. Graf, M. Philipp, O. Ricken, J. Stutzki, B. Vowinkel, M. C. Wiedner, C. Walther, M. Fischer, and J. Faist, "Phase locking of a 1.5 Terahertz quantum cascade laser and use as a local oscillator in a heterodyne HEB receiver," *Opt. Express* **17**(3), 1159–1168 (2009).
12. A. Danylov, N. Erickson, A. Light, and J. Waldman, "Phase locking of 2.324 and 2.959 terahertz quantum cascade lasers using a Schottky diode harmonic mixer," *Opt. Lett.* **40**(21), 5090–5092 (2015).
13. L. Consolino, A. Taschin, P. Bartolini, S. Bartolini, P. Cancio, A. Tredicucci, H. E. Beere, D. A. Ritchie, R. Torre, M. S. Vitiello, and P. De Natale, "Phase-locking to a free-space terahertz comb for metrological-grade terahertz lasers," *Nat. Commun.* **3**(1), 1040 (2012).
14. M. Ravaro, C. Manquest, C. Sirtori, S. Barbieri, G. Santarelli, K. Blary, J.-F. Lampin, S. Khanna, and E. Linfield, "Phase-locking of a 2.5 THz quantum cascade laser to a frequency comb using a GaAs photomixer," *Opt. Lett.* **36**(20), 3969–3971 (2011).
15. A. L. Betz, R. T. Boreiko, B. S. Williams, S. Kumar, Q. Hu, and J. L. Reno, "Frequency and phase-lock control of a 3 THz quantum cascade laser," *Opt. Lett.* **30**(14), 1837–1839 (2005).
16. A. A. Danylov, T. M. Goyette, J. Waldman, M. J. Coulombe, A. J. Gatesman, R. H. Giles, W. D. Goodhue, X. Qian, and W. E. Nixon, "Frequency stabilization of a single mode terahertz quantum cascade laser to the kilohertz level," *Opt. Express* **17**(9), 7525–7532 (2009).
17. J. R. Freeman, L. Ponnampalam, H. Shams, R. A. Mohandas, C. C. Renaud, P. Dean, L. Li, A. G. Davies, A. J. Seeds, and E. H. Linfield, "Injection locking of a terahertz quantum cascade laser to a telecommunications wavelength frequency comb," *Optica* **4**(9), 1059–1064 (2017).
18. A. Arie, S. Schiller, E. K. Gustafson, and R. L. Byer, "Absolute frequency stabilization of diode-laser-pumped Nd:YAG lasers to hyperfine transitions in molecular iodine," *Opt. Lett.* **17**(17), 1204–1206 (1992).
19. G. Galzerano, C. Svelto, E. Bava, and F. Bertinetto, "High-frequency-stability diode-pumped Nd:YAG lasers with the FM sidebands method and Doppler-free iodine lines at 532 nm," *Appl. Opt.* **38**(33), 6962–6966 (1999).
20. H. Richter, S. G. Pavlov, A. D. Semenov, L. Mahler, A. Tredicucci, H. E. Beere, D. A. Ritchie, and H.-W. Hübers, "Submegahertz frequency stabilization of a terahertz quantum cascade laser to a molecular absorption line," *Appl. Phys. Lett.* **96**(7), 071112 (2010).

21. F. Cappelli, I. Galli, S. Borri, G. Giusfredi, P. Cancio, D. Mazzotti, A. Montori, N. Akikusa, M. Yamanishi, S. Bartalini, and P. D. Natale, "Subkilohertz linewidth room-temperature mid-infrared quantum cascade laser using a molecular sub-doppler reference," *Opt. Lett.* **37**(23), 4811–4813 (2012).
22. Y. Ren, D. J. Hayton, J. N. Hovenier, M. Cui, J. R. Gao, T. M. Klapwijk, S. C. Shi, T.-Y. Kao, Q. Hu, and J. L. Reno, "Frequency and amplitude stabilized terahertz quantum cascade laser as local oscillator," *Appl. Phys. Lett.* **101**(10), 101111 (2012).
23. B. Wei, S. J. Kindness, N. W. Almond, R. Wallis, Y. Wu, Y. Ren, S. C. Shi, P. Braeuninger-Weimer, S. Hofmann, H. E. Beere, D. A. Ritchie, and R. Degl'Innocenti, "Amplitude stabilization and active control of a terahertz quantum cascade laser with a graphene loaded split-ring-resonator array," *Appl. Phys. Lett.* **112**(20), 201102 (2018).
24. M. Hempel, B. Röben, L. Schrottke, H.-W. Hübers, and H. T. Grahn, "Fast continuous tuning of terahertz quantum-cascade lasers by rear-facet illumination," *Appl. Phys. Lett.* **108**(19), 191106 (2016).
25. T. Alam, M. Wienold, X. Lü, K. Biermann, L. Schrottke, H. T. Grahn, and H.-W. Hübers, "Wideband, high-resolution terahertz spectroscopy by light-induced frequency tuning of quantum-cascade lasers," *Opt. Express* **27**(4), 5420–5432 (2019).
26. M. Wienold, B. Röben, L. Schrottke, R. Sharma, A. Tahraoui, K. Biermann, and H. T. Grahn, "High-temperature, continuous-wave operation of terahertz quantum-cascade lasers with metal-metal waveguides and third-order distributed feedback," *Opt. Express* **22**(3), 3334–3348 (2014).
27. H. M. Pickett, R. L. Poynter, E. A. Cohen, M. L. Delitsky, J. C. Pearson, and H. S. P. Müller, "Submillimeter, millimeter, and microwave spectral line catalog," *J. Quant. Spectrosc. Radiat. Transfer* **60**(5), 883–890 (1998).